Journal of Materials Chemistry C

ROYAL SOCIETY OF CHEMISTRY

PAPER

View Article Online
View Journal

Cite this: DOI: 10.1039/c9tc05374c

Improved charge transport in fused-ring bridged hemi-isoindigo-based small molecules by incorporating a thiophene unit for solution-processed organic field-effect transistors†

Guobing Zhang, *[ab] Ruikun Chen,[ab] Yue Sun,[ab] Boseok Kang,[c] Mingxiang Sun,[ab] Hongbo Lu, [ab] Longzhen Qiu, *[ab] Kilwon Cho [d] and Yunsheng Ding[b]

Received 30th September 2019,
Accepted 22nd November 2019

DOI: 10.1039/c9tc05374c

rsc.li/materials-c

Two acceptor–donor–acceptor small molecules based on a fused ring indacenodithieno[3,2-*b*]-thiophene (**IDTT**) as a donor, and hemi-isoindigo units, methyleneoxindole (**IDTT-MI**) and thienyl-methyleneoxindole (**IDTT-T-MI**) as acceptors were synthesized and characterized for application in solution-processed organic field-effect transistors. The incorporation of a thiophene bridge which extended the conjugation of the backbone maintained highly co-planar structures, and also endowed the small molecule with ordered crystalline structures and interconnected morphology. Consequently, **IDTT-T-MI**-based organic field-effect transistors exhibited a highest hole mobility of 0.80 $cm^2 V^{-1} s^{-1}$, which was the highest mobility for solution-processed hemi-isoindigo-based organic semiconductor materials.

1. Introduction

Organic semiconductor materials which contain polymers, oligomers, and small molecules have received tremendous attention in organic field-effect transistors (OFETs) due to their potential application in low-cost, light-weight, and flexible electronics.[1–3] Significant progress in OFETs has been achieved during the past years, with the hole and electron mobilities both surpassing 10 $cm^2 V^{-1} s^{-1}$, which has also promoted the synthesis of new constructing units for developing their new conjugated polymers and small molecules with excellent device performances.[4,5] Within the constructing block library for small molecules and conjugated polymers, imide- and lactam-containing dyes such as diketopyrrolopyrrole (DPP), isoindigo (ID), naphthalene diimide (NDI), and so on have been the most important electron-deficient units for constructing high-performance OFET semiconductors to date.[6–8] The ID unit which also possesses two lactam groups, has received particular attention in high-performance semiconductor materials for OFET and organic solar cell applications since Reynolds *et al.* first reported ID-based organic semiconductors.[9,10] ID has a symmetrical structure containing two hemi-isoindigo units, deep lowest unoccupied molecular orbital (LUMO)/highest occupied molecular orbital (HOMO) energy levels, large local dipole, excellent solubility *via* alkyl-substitution, and scalable synthesis with high yields,[11,12] all which endow a large quantity of molecular and polymeric ID-based materials with superior photoelectronic properties to develop rapidly.[13,14] For example, Chen reported a conjugated polymer based on ID as the acceptor and dithiophene as the donor, which exhibited a high field-effect mobility up to 8 $cm^2 V^{-1} s^{-1}$ with excellent air stability.[15] Therefore, ID has proven to be an effective electron-acceptor unit for the design and synthesis of semiconductors for organic electronic applications. It is well known that the ID unit is a twisted conjugated structure, with two hemi-isoindigo units rotating at a torsion angle of about 20° along the C–C double bond because of the steric interaction between the hydrogen atoms of the one hemi-isoindigo and the carbonyl oxygens on the other hemi-isoindigo unit.[16] The backbone structures with excellent coplanarity are considered to be beneficial for the charge transport.[17]

Based on the planar backbone requirements mentioned above, effective strategies were used to optimize the backbone coplanarity by designing ID derivatives. On the one hand,

[a] *Special Display and Imaging Technology Innovation Center of Anhui Province, State Key Laboratory of Advanced Display Technology, Academy of Opto-Electronic Technology, Hefei University of Technology, Hefei, 230009, P. R. China. E-mail: gbzhang@hfut.edu.cn, lzhqiu@hfut.edu.cn*

[b] *School of Chemistry and Chemical Engineering, Hefei University of Technology, Key Laboratory of Advance Functional Materials and Devices of Anhui Province, Hefei, 23009, P. R. China*

[c] *Department of Nano Engineering and SKKU Advanced Institute of Nanotechnology (SAINT), Sungkyunkwan University (SKKU), Suwon, 16419, Korea*

[d] *Department of Chemical Engineering, Pohang University of Science and Technology, Pohang, 37673, Korea*

† Electronic supplementary information (ESI) available. See DOI: 10.1039/c9tc05374c

thieno-ID, aza-ID, and halogen-substituted ID units were synthesized by replacing the outer benzene ring with thiophene, pyridine, and halogen-based rings,[18–20] respectively. The corresponding conjugated semiconductors based on the ID derivatives exhibited high mobility due to the improved backbone coplanarity. For example, Yu *et al.* reported aza-ID and its conjugated polymers by nitrogen substitution. The aza-ID possessed a highly planar structure and exhibited dihedral angles between a hemi-isoindigo unit of about 0°. Consequently, a high hole mobility up to 7 $cm^2 V^{-1} s^{-1}$ was obtained for OFET devices.[21] On the other hand, dithiophene, thienylethylene, and their derivatives were used as bridges instead of a double bond to connect the hemi-isoindigo unit.[22,23] The corresponding ID analogues not only possessed the extended conjugated core but also possessed a planar conjugated backbone because of the noncovalent interactions between S···O.[22] The small molecules and polymers based on these extended units have been extensively investigated for application in OFETs.[24,25] Nevertheless, the device performances were relatively low and the highest mobility was no more than 0.5 $cm^2 V^{-1} s^{-1}$ for both small molecules and polymers to date.[26] Therefore, further improving the charge transport mobility by designing new semiconductors based on the extension unit and investigating the relationship between their structures and properties in detail are still significant for OFET applications.

In this paper, a ladder-type arene, indacenodithieno[3,2-*b*]-thiophene (**IDTT**), was introduced between two hemi-isoindigo units, and then two new small molecules, named **IDTT-MI** and **IDTT-T-MI** (Scheme 1), were synthesized based on **IDTT** as the donor and methyleneoxindole (**MI**) and thienylmethyleneoxindole (**T-MI**) as acceptors for solution-processed OFET applications. **IDTT** has a heptacyclic ring with a planar structure and a large-plane conjugated center, which are in favor of the π-orbital overlap and charge transport mobility. Solution-processed OFET devices based on small molecules as the semiconducting layers, which were characterized under ambient conditions, exhibited hole transport characteristics. **IDTT-T-MI** had a highest mobility of 0.80 $cm^2 V^{-1} s^{-1}$ and an average mobility of 0.73 $cm^2 V^{-1} s^{-1}$ with an I_{on}/I_{off} ratio of over 10^5. The results indicate that the hemi-isoindigo small molecules based on a fused-ring are promising semiconductors for solution-processed OFET applications.

2. Results and discussion

Synthesis and characterization

The synthetic route to two small molecules is outlined in Scheme 1. 1-Hexyl-indoline-2,3-dione (**1**) was obtained by attaching the hexyl side chain to the lactam nitrogen atoms in the commercially available indoline-2,3-dione. The compound was reduced by hydrazine hydrate to form 1-hexyl-indoline-2-one (**2**). Then monomer **3** was synthesized using the Knoevenagel condensation reaction of 1-hexyl-indoline-2-one and 5-bromothiophene-2-carbaldehyde in the presence of weak basic conditions. Finally, two small molecules were synthesized *via* the Knoevenagel condensation reaction and the Stille reaction for **IDTT-MI** and **IDTT-T-MI**, respectively. The chemical structures of the small molecules were confirmed by nuclear magnetic resonance (NMR) and matrix-assisted laser desorption ionization time-of-flight mass spectrometry (MALDI-TOF-MS). The ^1H spectrum of **IDTT-T-MI** was measured under high-temperature conditions (90 °C), and both ^{13}C spectra were not obtained due to the limited solubility. The thermal properties of the two small molecules were investigated by

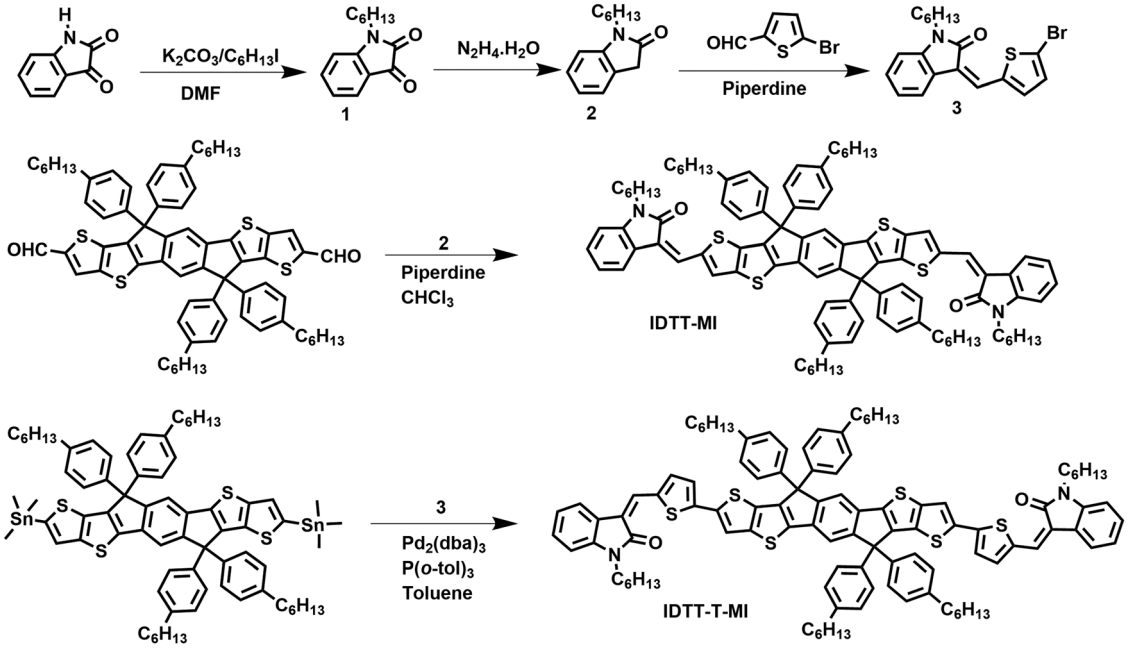

Scheme 1 Synthetic route to two small molecules.

thermogravimetric analysis (TGA) under a nitrogen atmosphere (Fig. S1, ESI†). High decomposition temperatures (T_d) with 5% weight loss of both over 400 °C were obtained, indicating excellent thermal stability for the two small molecules.

Optical and electrochemical properties

The optical properties of two small molecules were investigated by UV-vis absorption spectroscopy. The normalized absorption spectra characterized in chloroform solutions, on drop-cast thin films, and annealed films are shown in Fig. 1. In solution, **IDTT-T-MI** exhibited an absorption maximum at ~558 nm (Table 1), which was red-shifted by *ca.* 5 nm compared with **IDTT-MI** (553 nm). Moreover, **IDTT-T-MI** showed a significant increase of the 0–0 vibrational peak. As expected, the two small molecules showed apparent red-shifts and broadened absorption spectra in thin films. For example, the absorption maxima at 558 nm in solution was red-shifted to 600 nm with significant shoulders emerging at 520 and 558 nm for the thin film of **IDTT-T-MI**, suggesting strong intermolecular interactions in the solid state.[17] Relative to the absorption of the **IDTT-MI** film, **IDTT-T-MI** displayed distinctly red-shifted absorption peaks with a red shift of *ca.* 20 nm. The significant bathochromic-shift for **IDTT-T-MI** may be attributed to the extended effective-conjugation-length by incorporating the thiophene bridge between the hemi-isoindigo and fused ring units. Annealing the films led to further red-shifts of about 5 nm for the absorption maxima of **IDTT-T-MI**, albeit slightly, indicating the greater planarization and the improvement of the molecule ordering.[27] The optical band gaps of **IDTT-MI** and **IDTT-T-MI** are 1.97 and 1.94 eV, respectively, which were calculated from the thin film absorption onset (628 and 648 nm).

The electrochemical properties of the two small molecules were investigated using cyclic voltammetry (CV). As shown in Fig. 2a, the reduction and oxidation peaks of **IDTT-MI** and **IDTT-T-MI** were located at −1.23/0.63 and −1.15/0.59 eV, respectively. According to the equation (Table 1), the LUMO and HOMO energy levels were calculated to be −3.52/−5.38 eV and −3.60/−5.34 eV for **IDTT-MI** and **IDTT-T-MI**, respectively, indicating that the two small molecules might be potential p-type transport materials in OFET devices when a suitable metal is used as the electrode. The incorporation of a thiophene bridge and extension of the effective-conjugation-length resulted in a slight decrease in the LUMO energy level and an increase in the HOMO energy level. Consequently, **IDTT-T-MI** exhibited a narrower bandgap (1.74 eV) than **IDTT-MI** (1.86 eV).

Density functional theory (DFT) calculations at the B3LYP/6-31G(d) level were also used to investigate the electronic structures of **IDTT-MI** and **IDTT-T-MI**. All the hexyl side chains in small molecules were replaced with methyl groups, and the corresponding calculation results are shown in Fig. 2b and Fig. S2 (ESI†). **IDTT-MI** exhibited a small dihedral angle of 0.1° between the fused ring and the hemi-isoindigo unit, implying a coplanar backbone for **IDTT-MI** probably because of the intramolecular interactions. Upon incorporating the thiophene bridge between the hemi-isoindigo and thiophene units, the dihedral angle dropped to 0.05°, indicating minimal torsional effects. Moreover, the other dihedral angle for **IDTT-T-MI** between the fused ring and the thiophene unit was calculated to be 0.5°. These results indicate that the incorporation of the thiophene bridge did not exert a detrimental effect and the extended conjugation also possessed a planar backbone, which is beneficial for the ordered aggregation, thus enhancing the charge-carrier transport. The S···O distance was calculated to

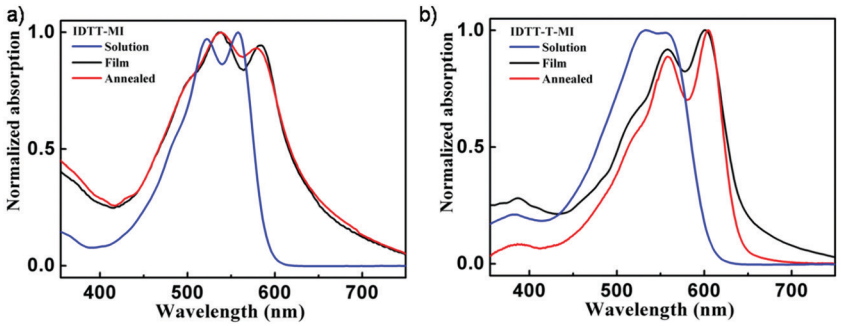

Fig. 1 UV-vis absorption of (a) **IDTT-MI** and (b) **IDTT-T-MI** in chloroform solution and thin films with and without annealing.

Table 1 Decomposition temperatures, optical properties, and energy levels of two small molecules

Molecule	T_d[a] [°C]	λ_{max} [nm] Solution	λ_{max} [nm] Film	λ_{onset} [nm]	E_g^{opt}[b] [eV]	E_{HOMO}[c] [eV]	E_{LUMO}[c] [eV]	E_g^{cv} [eV]
IDTT-MI	406	522/553	538/584	628	1.97	−5.38	−3.52	1.86
IDTT-T-MI	414	532/558	558/600	640	1.94	−5.34	−3.60	1.74

[a] The 5 wt% loss temperature. [b] $E_g^{opt} = 1240/\lambda_{onset}$. [c] HOMO = $-(4.75 + E_{onset}^{ox})$ and LUMO = $-(4.75 + E_{onset}^{red})$; the redox Fc/Fc^+ was located at 0.05 V related Ag/Ag^+.

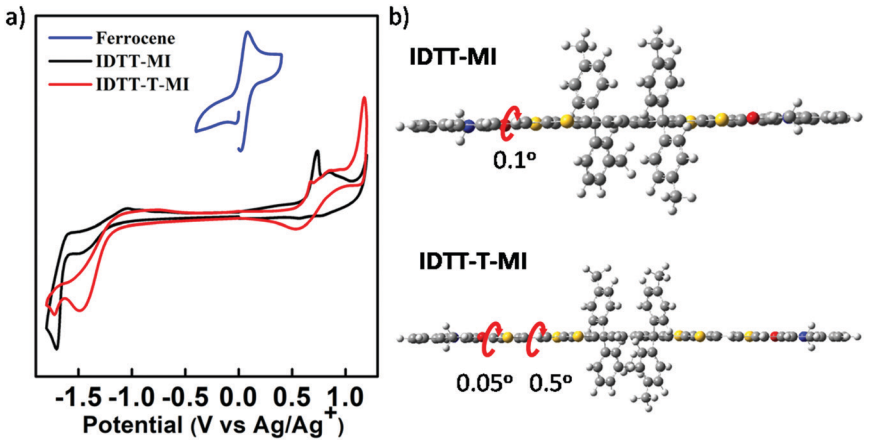

Fig. 2 (a) Cyclic voltammogram and (b) the optimized structures according to the DFT calculation at the B3LYP/6-31G(d) level.

be 2.79 Å (Fig. S2, ESI†), shorter than the combined van der Waals radii of *ca.* 3.32 Å, indicative of the existence of intramolecular S···O interactions.[28]

Field-effect properties

The field-effect properties of the **IDTT-MI** and **IDTT-T-MI** were investigated using a bottom-gate/top-contact (BG/TC) configuration. The OFET devices were fabricated in a glovebox and characterized under ambient conditions. The corresponding device performances are summarized in Table S1 (ESI†). First, the semiconductor films were spin-coated from a conventional halogenated solution (6 mg mL^{-1}). No field-effect performances were observed for both as-prepared OFETs, probably because of the amorphous structures for the non-annealing (N/A) films. The two small molecules displayed typical hole transport characteristics after annealing at different temperatures ranging from 180 to 260 °C (Fig. 3 and Fig. S3, ESI†). In the case of **IDTT-MI**, the device was optimized *via* thermal annealing and exhibited a maximum hole mobility (μ_{max}) of 0.036 $cm^2\ V^{-1}\ s^{-1}$ and an average mobility (μ_{avg}) of 0.023 $cm^2\ V^{-1}\ s^{-1}$, with an current ON/OFF ratio (I_{ON}/I_{OFF}) of over 10^5 and a threshold voltage (V_{th}) of −8.8 V. With the incorporation of the thiophene bridge into the backbone, **IDTT-T-MI** exhibited much-improved device performances at least one order of magnitude compared to **IDTT-MI** without thiophene bridge. After annealing at 180 °C, the hole mobility reached 0.26 $cm^2\ V^{-1}\ s^{-1}$, and when the annealing temperature was further increased to 210 °C, the hole mobility continued to reach 0.37 $cm^2\ V^{-1}\ s^{-1}$ (Fig. S3, ESI†). The OFET devices exhibited optimized performances when annealed at 240 °C, and **IDTT-T-MI** showed μ_{max} as high as 0.80 $cm^2\ V^{-1}\ s^{-1}$ with a high I_{ON}/I_{OFF} ratio (over 10^5) and a low V_{th} (−4.8 V, Fig. 3b). Further increase in the annealing temperature above 240 °C resulted in lower device performances. For instance, the μ_{max} decreased to 0.30 $cm^2\ V^{-1}\ s^{-1}$ for the 260 °C-annealing devices. **IDTT-T-MI** based devices displayed very low V_{th}, which is beneficial for fabricating low-power-consumption devices. Moreover, all the output curves showed negligible hysteresis even at a high gate voltage (V_{GS} = 100 V). These results indicated

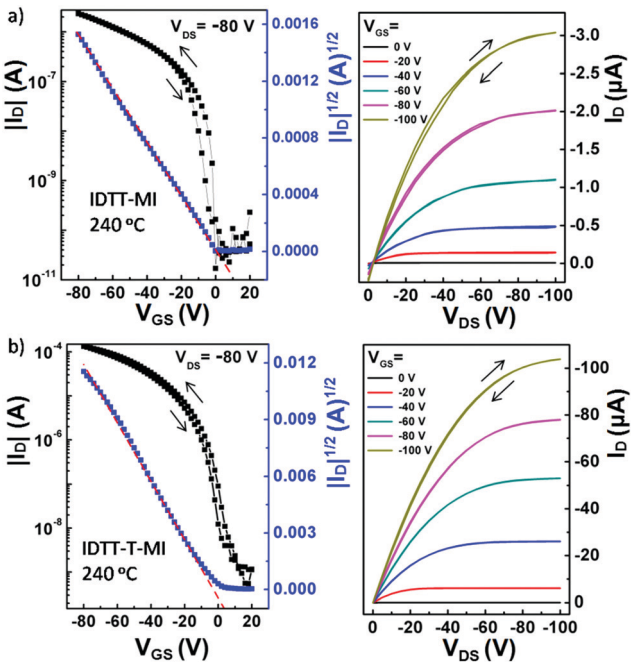

Fig. 3 The transfer and output characteristics of OFETs for the two small molecules. The films were spin-coated from chloroform solution.

that **IDTT-T-MI** should be a high-performance semiconductor which exhibited much higher hole mobilities compared to those of **IDTT-MI** under the same conditions. The chemical structures of the two small molecules are different in the thiophene bridge, which not only extends the conjugation length but also enhances the intramolecular interactions,[29–31] which both probably result in different crystal structures and thin-film morphology.

It is well known that the chloroform used above is not an environmentally-friendly solvent. To date, most OFET devices are fabricated using a halogenated solvent, which may result in serious environmental issues. Herein, the nonhalogenated solvent, tetrahydrofuran (THF), was used for fabricating **IDTT-T-MI**-based devices. The device results are summarized

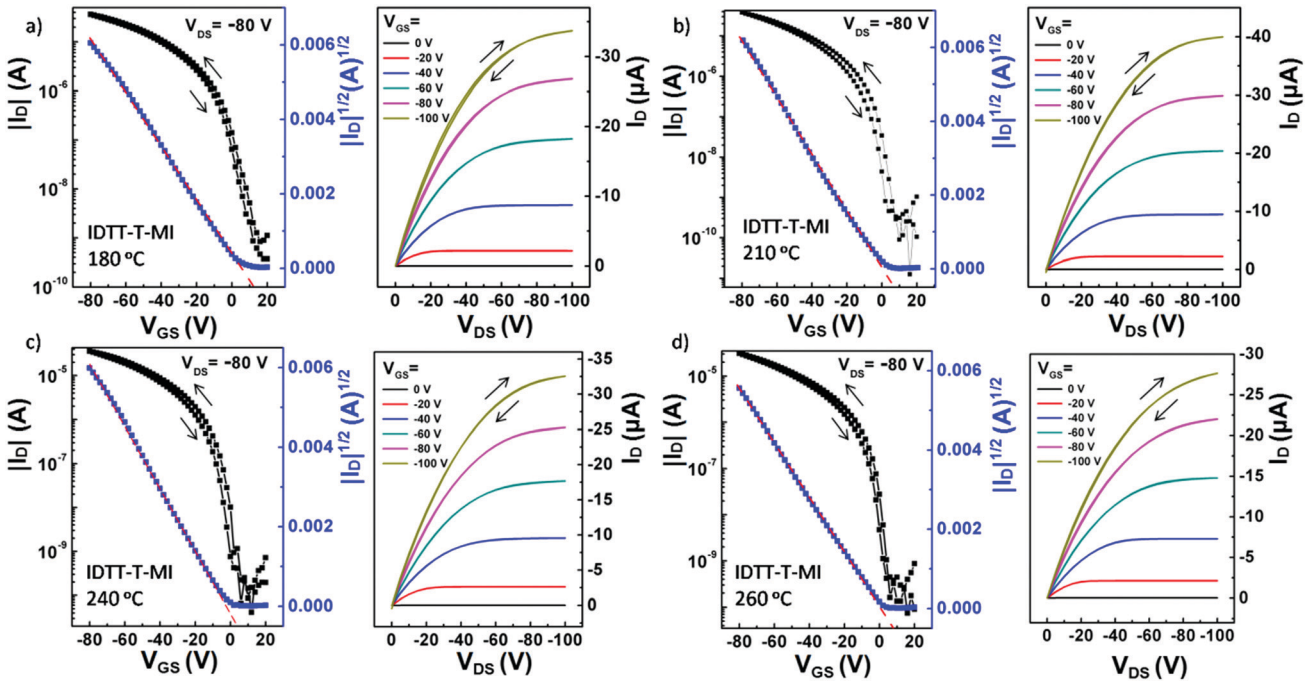

Fig. 4 The transfer and output characteristics of OFETs for the **IDTT-T-MI**. The films were spin-coated from tetrahydrofuran (THF) solution.

in Table S1 (ESI†), and the transfer/output curves are shown in Fig. 4. **IDTT-T-MI**-based OFET devices also exhibited excellent performances even if the nonhalogenated solvent was used. The devices fabricated from the THF solvent showed a similar level of performance compared to those from the chloroform solvent (Table S1, ESI†). A highest hole mobility of 0.32 $cm^2 V^{-1} s^{-1}$ and an average mobility of 0.27 $cm^2 V^{-1} s^{-1}$ were obtained, with a high I_{ON}/I_{OFF} ratio of over 10^5 and a low V_{th} of below −6 V after annealing at 210 °C.

Crystallinity and morphology

Grazing-incidence X-ray diffraction (GIXD) and atomic force microscopy (AFM) were employed in this work to investigate the crystal structure and microstructure of the two small molecule thin-films. The 2D-GIXD patterns of the annealing films are shown in Fig. 5. **IDTT-MI** showed strong diffraction peaks at 0.36 $Å^{-1}$ corresponding to (001) and also showed a very weak second-order diffraction peak at 0.38 $Å^{-1}$ corresponding to (002) along the out-of-plane (Fig. S5, ESI†). Upon incorporating the thiophene bridge, **IDTT-T-MI** exhibited an obvious enhanced diffraction peak (002) as well as a strong peak (001). These results indicated that the incorporation of the thiophene bridge into the backbone endowed **IDTT-T-MI** with a more ordered lamellar crystalline structure. The corresponding d_{001} spacings of two small molecules were calculated to be 17.4 Å for **IDTT-MI** and 16.4 Å for **IDTT-T-MI**, suggesting that there may be at least in **IDTT-T-MI** interdigitation of the alkyl chains along the lamella packing direction. Moreover, by using the 1D intensity profiles of the 2D-GIXD pattern, the d_{100} and d_{010} spacings were found to be 14.5/8.2 Å and 17.0/8.0 Å for **IDTT-MI** and **IDTT-T-MI** (Fig. S6, ESI†), respectively. According to the verification from the DFT-simulated structure, the molecular lengths of **IDTT-MI** and **IDTT-T-MI**, which along the direction of the molecular long axis, were calculated to be approximately

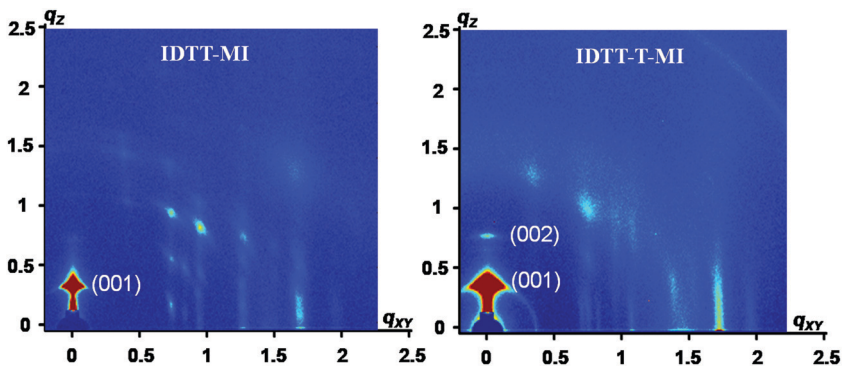

Fig. 5 GIXD patterns of two small molecules after thermal annealing at optimized temperatures.

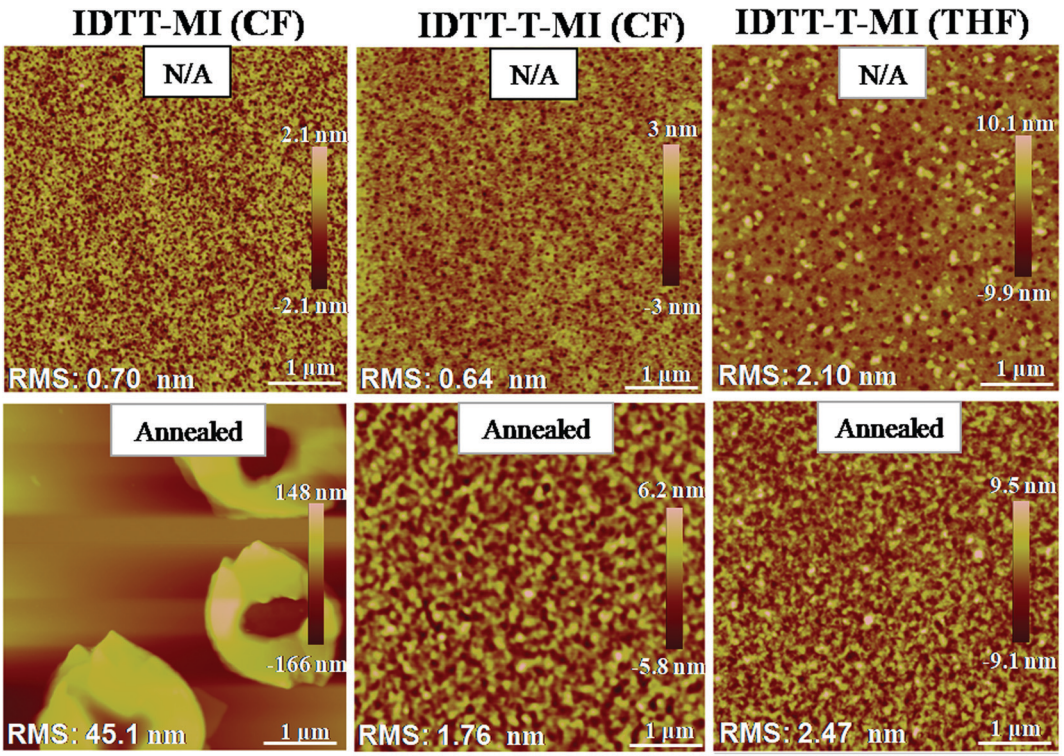

Fig. 6 AFM height images of two small molecule films spin-coated from different solutions (CF and THF) with and without annealing.

25.0 and 35.5 Å (Fig. S7, ESI†) respectively, indicating that there should be an overlap along the molecular long axis for the two small molecules. The solid-state structures of **IDTT-MI** and **IDTT-T-MI** were obtained from GIXD and simulated calculations, in which the estimated π–π stacking distance is half of d_{010} distances, approximately 4.1 and 4.0 Å for **IDTT-MI** and **IDTT-T-MI**, respectively. **IDTT-T-MI** had smaller π–π distances as well as more ordered lamellar crystalline structures compared to **IDTT-MI**, which may both contribute to the higher hole mobilities for **IDTT-T-MI** based devices.

The AFM height images of the as-spun and thermally annealed thin-films are shown in Fig. 6. The as-spun films processed from chloroform solution both displayed amorphous-like morphology and the whole AFM images exhibited a smooth surface with no obvious crystalline region (Fig. 6). In contrast, the **IDTT-T-MI** film spin-coated from THF solution exhibited a fine crystal structure throughout the thin-film. However, the **IDTT-T-MI** crystallites are of small size and separate from each other. As a result, the discontinuous morphology may be difficult to form an efficient pathway for charge carrier transport. These results from the as-spun films well explained why the OFET devices without annealing did not exhibit any field-effect. After annealing, relatively large crystals formed in the **IDTT-MI** film while obvious dewetting was also observed, and this may be responsible for the low mobility. Moreover, the **IDTT-MI** film showed a seriously rough surface with a too large root mean square roughness (RMS) of over 45 nm, which may also result in poor interfacial contact between the thin-film and the electrode, and is thus also unfavorable for charge transport. **IDTT-T-MI** films processed from chloroform and THF solution both exhibited continuous and nanofibrillar crystal structures over the entire area. The well-interconnected network could form a highly efficient pathway for charge transport, which may be beneficial for the high field-effect mobility obtained for the annealing devices. In short, according to the results mentioned above, **IDTT-MI** exhibited low field-effect performances, which are mainly ascribed to the poor film-forming properties, such as the dewetting film and too rough surface. The high hole mobility for **IDTT-T-MI** may be attributed to the extended conjugation, excellent crystal structure, close π–π stacking, and well-interconnected morphology.

3. Conclusions

Two new A–D–A small molecules (**IDTT-MI** and **IDTT-T-MI**) based on a fused ring and a hemi-isoindigo unit were synthesized for application in solution-processed OFETs. The incorporation of a thiophene bridge into the backbone not only extended the conjugation length but also maintained the highly co-planar structure. **IDTT-T-MI** showed more ordered crystalline structure, closer π–π stacking, and much better-interconnected morphology compared to **IDTT-MI** without a thiophene bridge. Consequently, OFET devices based on **IDTT-T-MI** exhibited a high hole mobility of over 0.80 $cm^2\ V^{-1}\ s^{-1}$ with a high I_{ON}/I_{OFF} ratio and a low V_{th}. Moreover, the film spin-coated from a nonhalogenated solvent (THF) also displayed excellent field-effect performances with a mobility as high as 0.32 $cm^2\ V^{-1}\ s^{-1}$. These results indicated that the fused

ring-connected hemi-isoindigo small molecules are promising semiconductors for solution-processed OFET applications.

Conflicts of interest

There are no conflicts to declare.

Acknowledgements

This study was supported by the National Natural Science Foundation of China (NSFC, Grants 51573036 and 51703047), the Fundamental Research Funds for the Central Universities (Grant No. JZ2018HGPB0276), the Distinguished Youth Foundation of Anhui Province (1808085J03), Anhui Provincial Natural Science Foundation (1908085MF200), and the Open Foundation of State Key Laboratory of Electronic Thin Films and Integrated Devices (KFJJ201804). The authors thank 3C beamlines (the Pohang Accelerator Laboratory in Korea) for providing the beam time.

Notes and references

1 A. F. Paterson, S. Singh, K. J. Fallon, T. Hodsden, Y. Han, B. C. Schroeder, H. Bronstein, M. Heeney, L. McCulloch and T. D. Anthopoulos, *Adv. Mater.*, 2018, **30**, 1801079.
2 Y. Wang and T. Michinobu, *J. Mater. Chem. C*, 2018, **6**, 10390–10410.
3 L. X. Shi, Y. L. Guo, W. P. Huand and Y. Q. Liu, *Mater. Chem. Front.*, 2017, **1**, 2423–2456.
4 H. W. Luo, C. M. Yu, Z. T. Liu, G. X. Zhang, H. Geng, Y. P. Yi, K. Broch, Y. Y. Hu, A. Sadhanala, L. Jiang, P. L. Qi, Z. X. Cai, H. Sirringhaus and D. Q. Zhang, *Sci. Adv.*, 2016, **2**(5), e1600076.
5 J. H. Dou, Y. Q. Zheng, Z. F. Yao, Z. A. Yu, T. Lei, X. X. Shen, X. Y. Luo, J. L. Sun, S. D. Zhang, Y. F. Ding, G. C. Han, Y. P. Yi, J. Y. Wang and J. Pei, *J. Am. Chem. Soc.*, 2015, **137**, 15947–15956.
6 I. Kang, H. J. Yun, D. S. Chung, S. K. Kwon and Y. H. Kim, *J. Am. Chem. Soc.*, 2013, **135**, 14896–14899.
7 B. Kang, R. Kim, S. B. Lee, S. K. Kwon, Y. H. Kim and K. Cho, *J. Am. Chem. Soc.*, 2016, **138**, 3679–3686.
8 Y. Liu, F. F. Wang, J. H. Chen, X. H. Wang, H. B. Lu, L. Z. Qiu and G. B. Zhang, *Macromolecules*, 2018, **51**, 370–378.
9 J. G. Mei, K. R. Graham, R. Stalder and J. R. Reynolds, *Org. Lett.*, 2010, **12**, 660–663.
10 G. B. Zhang, Y. Y. Fu, Z. Y. Xie and Q. Zhang, *Macromolecules*, 2011, **44**, 1414–1420.
11 D. H. Kim, A. L. Ayzner, A. L. Appleton, K. Schmidt, J. G. Mei, M. F. Toney and Z. N. Bao, *Chem. Mater.*, 2013, **25**, 431–440.
12 L. A. Estrada, R. Stalder, K. A. Abboud, C. Risko, J. L. Bredas and J. R. Reynolds, *Macromolecules*, 2013, **46**, 8832–8844.
13 T. Lei, J. H. Dou and J. Pei, *Adv. Mater.*, 2012, **24**, 6457–6461.
14 J. G. Mei, D. H. Kim, A. L. Ayzner, M. F. Toney and Z. N. Bao, *J. Am. Chem. Soc.*, 2011, **133**, 20130–20133.
15 H. C. Wu, C. C. Hung, C. W. Hong, H. S. Sun, J. T. Wang, G. Yamashita, T. Higashihara and W. C. Chen, *Macromolecules*, 2016, **49**, 8540–8548.
16 P. Deng and Q. Zhang, *Polym. Chem.*, 2014, **5**, 3298–3305.
17 G. B. Zhang, Y. Zhao, B. Kang, S. Park, J. F. Ruan, H. B. Lu, L. Z. Qiu, Y. S. Ding and K. Cho, *Chem. Mater.*, 2019, **31**, 2027–2035.
18 R. S. Ashraf, A. J. Kronemeijer, D. I. James, H. Sirringhaus and I. M. Culloch, *Chem. Commun.*, 2012, **48**, 3939–3941.
19 W. Yue, M. Nikolka, M. F. Xiao, A. Sadhanala, C. B. Nielsen, A. J. P. White, H. Y. Chen, A. Onwubiko, H. Sirringhaus and I. M. Cullochad, *J. Mater. Chem. C*, 2016, **4**, 9704–9710.
20 T. Lei, J. H. Dou, Z. J. Ma, C. H. Yao, C. J. Liu, J. Y. Wang and J. Pei, *J. Am. Chem. Soc.*, 2012, **134**, 20025–20028.
21 J. Y. Huang, Z. P. Mao, Z. H. Chen, D. Gao, C. Y. Wei, W. F. Zhang and G. Yu, *Chem. Mater.*, 2016, **28**, 2209–2218.
22 S. G. Li, Z. C. Yuan, J. Y. Yuan, P. Deng, Q. Zhang and B. Sun, *J. Mater. Chem. A*, 2014, **2**, 5427–5433.
23 J. Wu, J. D. Chen, H. Huang, S. X. Li, H. W. Wu, C. Hu, J. X. Tang and Q. Zhang, *Macromolecules*, 2016, **49**, 2145–2152.
24 W. F. Zhang, N. H. Zheng, C. Y. Wei, J. Y. Huang, D. Gao, K. L. Shi, J. Xu, D. H. Yan, Y. C. Han and G. Yu, *Polym. Chem.*, 2016, **7**, 1413–1421.
25 T. Wu, C. M. Yu, Y. L. Guo, H. T. Liu, G. Yu, Y. Fang and Y. Q. Liu, *J. Phys. Chem. C*, 2012, **116**, 22655–22662.
26 Y. K. Zhou, S. Y. Zhang, W. F. Zhang, J. Y. Huang, C. Y. Wei, H. Li, L. P. Wang and G. Yu, *Macromolecules*, 2018, **51**, 7093–7103.
27 F. C. Spano, *Acc. Chem. Res.*, 2010, **43**, 429–439.
28 S. Alvarez, *Dalton Trans.*, 2013, **42**, 8617–8636.
29 J. Y. Wang, W. Wang, X. H. Wang, Y. Wu, Q. Q. Zhang, C. Q. Yan, W. Ma, W. You and X. W. Zhang, *Adv. Mater.*, 2017, **29**, 1702125.
30 X. Song, N. Gasparini, M. M. Nahid, H. Chen, S. M. Macphee, W. M. Zhang, V. Norman, C. H. Zhu, D. Bryant, H. Ade, I. McCulloch and D. Baran, *Adv. Funct. Mater.*, 2018, **28**, 1802895.
31 B. Y. Jia, S. X. Dai, Z. F. Ke, C. Q. Yan, W. Ma and X. W. Zhang, *Chem. Mater.*, 2017, **30**, 239.